JCTC Journal of Chemical Theory and Computation

Quantum Electronic Structure

Simple modifications of the SCAN meta-generalized gradient approximation functional

Pal Daniel Mezei, Gabor I. Csonka, and Mihaly Kallay

J. Chem. Theory Comput., **Just Accepted Manuscript** • DOI: 10.1021/acs.jctc.8b00072 • Publication Date (Web): 22 Mar 2018

ACS Publications

is published by the American Chemical Society. 1155 Sixteenth Street N.W., Washington, DC 20036

Simple modifications of the SCAN meta-generalized gradient approximation functional

Pál D. Mezei,[1*] Gábor I. Csonka[2], and Mihály Kállay[1]
[1] MTA-BME Lendület Quantum Chemistry Research Group, Department of Physical Chemistry and Materials Science, Budapest University of Technology and Economics, H-1521 Budapest, Hungary
[2] Department of Inorganic and Analytical Chemistry, Budapest University of Technology and Economics, H-1521 Budapest, Hungary
[*] E-mail: mezei.pal@mail.bme.hu

Abstract

We analyzed various possibilities to improve upon the SCAN meta-generalized gradient approximation density functional obeying all know properties of the exact functional which can be satisfied at this level of approximation. We examined the necessity of locally satisfying a strongly tightened lower bound for the exchange energy density in single-orbital regions, the nature of the error cancellation between the exchange and correlation parts in two-electron regions, and the effect of the fourth-order term in the gradient expansion of the correlation energy density. We have concluded that the functional can be modified to separately reproduce the exchange and correlation energies of the helium atom by locally releasing the strongly tightened lower bound for the exchange energy density in single-orbital regions, but this leads to an unbalanced improvement in the single-orbital electron densities. Therefore, we decided to keep the $F_X \leq 1.174$ exact condition for any single-orbital density, where F_X is the exchange enhancement factor. However, we observed a general improvement in the single-orbital electron densities by revising the correlation functional form to follow the second-order gradient expansion in a wider range. Our new revSCAN functional provides more accurate atomization energies for the systems with multi-reference character compared to the SCAN functional. The non-local VV10 dispersion-corrected revSCAN functional yields more accurate non-covalent interaction energies than the VV10-corrected SCAN functional. Furthermore, its global hybrid version with 25% of exact exchange called revSCAN0 performs generally better than the similar SCAN0 for reaction barrier heights. We also analyzed here the possibility of the construction of a local hybrid from the SCAN exchange and a specific locally bounded non-conventional exact exchange energy density. We predict compatibility problems since this non-conventional exact exchange energy density does not really obey the strongly tightened lower bound for the exchange energy density in single-orbital regions.

Introduction

Semi-local density functional approximations are widely-used cost-efficient tools in quantum chemistry.[1,2] They can be considered as systematic improvements upon the local density approximation (LDA)[3,4] with well understood error cancellation between the exchange and correlation parts.[5,6] Most semi-local functionals are engineered by empirical fitting[7,8] and/or constraint satisfaction.[9,10] We briefly discuss here the milestones of the development of non-empirical semi-local functionals that were constructed by constraint satisfaction.

Preserving the exactness for the homogeneous electron gas, several other exact constraints can be satisfied on the generalized gradient approximation (GGA) level.[11] The negativity of the exchange energy is satisfied if the exchange enhancement factor (F_X) is positive because the LDA exchange energy density is negative. The Lieb-Oxford bound on the exchange ($F_X \leq 1.804$) is certainly satisfied globally if the exchange energy density locally obeys this lower bound for any possible density.[12] In the slowly-varying

limit, the exchange energy density can be constructed to follow the second-order gradient expansion.[13] The spin-polarized exchange functional can be obtained from the spin-unpolarized one by the exact spin-scaling.[14] The exchange functional follows the exact uniform density scaling because the LDA exchange functional follows the uniform density scaling, and all the ingredients in the exchange enhancement factor are invariant under the uniform density scaling. The non-positivity of the correlation energy density can also be easily satisfied. In the slowly-varying limit, it can be constructed to follow the second-order gradient expansion.[15] In the rapidly-varying limit, the correlation can be made to vanish. Under uniform density scaling to the high-density limit, the gradient correction can be made to cancel the logarithmic singularity of the LDA correlation and scale to a constant.[16] The GGA exchange-correlation energy is naturally size-extensive since it contains only semi-local information. Furthermore, inherently from the LDA method, it is more or less independent of the relative spin-polarization in the low-density (strong-interaction) limit.[17]

The limitations of the GGA functional form can be well represented by two different non-empirical GGA functionals both obeying the Lieb-Oxford bound for the exchange and satisfying the second-order gradient expansion of the exchange. The PBEsol functional[18] with a quite flat exchange enhancement factor deviating early from the second-order gradient expansion gives fairly accurate lattice constants for solids but inaccurate atomization energies for molecules. In contrast, the RGE2 functional,[19] which follows the second-order gradient expansion of the exchange in a wider range provides somewhat better atomization energies but worse lattice constants. In the literature, many attempts show that the GGA functional form can be fine-tuned for a given property only at the expense of other properties.[20,21,22,23,24,25]

On the meta-GGA level,[26] one can preserve all the exact constraints satisfied on the GGA level and also add new ones. For example, the TPSS functional[27] still obeys the Lieb-Oxford bound on the exchange but it also uses the positively defined kinetic energy density of the Kohn-Sham orbitals to satisfy the fourth-order gradient expansion of the exchange[28] and to make the correlation part one-electron self-interaction free. This functional represents well that good atomization energies and lattice constants can be obtained at the same time on the meta-GGA level. This can be attributed partially to the freedom from one-electron self-correlation, and partially to the feature that the TPSS exchange-correlation energy is independent of the relative spin polarization in the low-density limit by construction.[29]

A strongly tightened lower bound on the exchange energy was rigorously derived for single-orbital densities (which means an upper bound on the exchange enhancement factor in the spin-unpolarized or two-electron case: $F_X \leq 1.174$),[30] which has opened a new class of meta-GGA functionals. Such functionals obeying this tighter lower bound on the exchange are the SCAN[31] and MVS[32] functionals. Among these, the SCAN functional obeys all known properties of the exact exchange-correlation functional which can be satisfied on the semi-local level. In addition to the above discussed exact constraints, the SCAN exchange scales to a negative constant under one-dimensional non-uniform density scaling to the high-density limit.[33,34] The SCAN correlation was also revised to be less incorrect for the non-uniform density scaling.[33,34] Furthermore, the SCAN exchange-correlation gives back the static linear response of the uniform electron gas and respects the general Lieb-Oxford bound ($F_{XC} \leq 1.804$, where F_{XC} is the exchange-correlation enhancement factor)[12] and a tighter Lieb-Oxford bound for two-electron densities ($F_{XC} \leq 1.671$).[31] Although the SCAN functional was not fitted to any bonded system, several tests show the predictive power of the applied exact constraints. The SCAN functional with D3(BJ)[35] dispersion correction has been reported to be the best-performing method among all the examined dispersion-corrected semi-local density functional methods for the extensive molecular energetics database, GMTKN55,[36] as well as for molecular geometries.[37] It also performs well in condensed matter physics: it captures the density difference between liquid water and solid ice,[38]

predicts accurately the energy difference in the semiconductor-metal phase transition of crystalline silicon, and distinguishes between diverse bond types in ferroelectric and multiferroic materials.[39]

SCAN is constructed from a functional form with parameters chosen to satisfy exact constraints (bounds, scaling relations, limits, *etc.*) and appropriate norms (systems for which the form can be exact, or nearly exact, such as the uniform electron gas or atoms). Here we explore a re-parametrization which allows a violation of the tight lower bound on the exchange energy for all one- and two-electron densities, but ultimately abandon it as unproductive. Instead, we preserve all the exact constraints, but revise the form of the correlation term and re-fit some parameters to atomization energies of molecules. This is a convenient choice for us, although it is counter to the SCAN objective to predict bonds without fitting to them.

Theory and computational details

In this paper, we use the following main variables: the α and β spin-densities $n_\uparrow$ and $n_\downarrow$, the total electron density $n = n_\uparrow + n_\downarrow$, the Wigner-Seitz radius $r_S = (4\pi\, n/3)^{-1/3}$, the relative spin-polarization $\zeta = (n_\uparrow - n_\downarrow)/(n_\uparrow + n_\downarrow)$, the spin-scaling factor $\phi = [(1+\zeta)^{2/3} + (1-\zeta)^{2/3}]/2$, the reduced gradient in the exchange $s = |\nabla n|/[2(3\pi^2)^{1/3} n^{4/3}]$, the reduced gradient in the correlation $t = (3\,\pi^2/16)^{1/3}\, s/(\phi r_S{}^{1/2})$, and $\alpha = (\tau - \tau_w)/\tau_{unif}$, where $\tau = \sum_{i,\sigma}^{occ} |\nabla \psi_{i,\sigma}|^2/2$ is the positively-defined kinetic energy density of the occupied Kohn-Sham orbitals (summed for all the i occupied orbitals and σ spins), $\tau_w = |\nabla n|^2/8\, n$ is the von Weizsäcker kinetic energy density, and $\tau_{unif} = (3/10)(3\pi^2)^{2/3} n^{5/3} d_S(\zeta)$ is the kinetic energy density of the homogeneous electron gas with $d_S(\zeta) = [(1+\zeta)^{5/3} + (1-\zeta)^{5/3}]/2$. Furthermore, we define two auxiliary variables: $A_1 = \beta_1(r_S)/\gamma w_1$ and $\chi_\infty(\zeta) = (3\pi^2/16)\beta(r_S \to \infty)\, \phi/[c_X(\zeta) - f_0]$, where $c_X(\zeta) = -[3/(4\pi)](9\,\pi/4)^{1/3} d_X(\zeta)$, $f_0 = -0.9$, $\chi_\infty(\zeta = 0) = 0.128026$, and the electron density dependent coefficient of the second-order term in the gradient expansion of the correlation is $\beta_1(r_S) = 0.066725\, \frac{1+0.1 r_S}{1+0.1778 r_S}$.

The original functional form of SCAN can be reviewed in ref 31, we present here only our modifications on the original functional form. The function g in the SCAN correlation [$g^{SCAN}(At^2) = 1/(1+4At^2)^{1/4}$, $g_\infty^{SCAN}(\zeta, s) = 1/(1+4\chi_\infty s^2)^{1/4}$] has a non-zero fourth-order term in its Taylor series in contrast to the g function in PBE [$g^{PBE}(At^2) = (1 + At^2 + A^2t^4)^{-1}$] and deviates from $1 - At^2$ more rapidly. Hence due to its fourth-order term, the SCAN correlation energy density deviates from the second-order gradient expansion more rapidly than the PBE correlation. We propose here a revised version of the SCAN correlation using a modified g function with zero fourth-order term in its Taylor series.

$$g^{mod}(At^2) = \frac{1}{2(1+8At^2)^{1/4}} + \frac{1}{2(1+80A^2t^4)^{1/8}} \quad (1)$$

$$g_\infty^{mod}(\zeta, s) = \frac{1}{2(1+8\chi_\infty s^2)^{1/4}} + \frac{1}{2(1+80\chi_\infty^2 s^4)^{1/8}} \quad (2)$$

Thus, we restore the small At^2 behavior of g^{PBE} in a wider range preserving the large At^2 behavior of g^{SCAN} (Figure 1). This way, the values of the b_{1C}, b_{2C}, and b_{3C} parameters in the single-orbital LDA part have to be chosen to the new functional form. Furthermore, the following derivatives were used for the revised SCAN correlation in place of the corresponding derivatives in the original SCAN implementation.

$$\frac{\partial g^{mod}(At^2)}{\partial A} = \frac{-2t^2}{2(1+8At^2)^{5/4}} + \frac{-20At^4}{2(1+80A^2t^4)^{9/8}} \quad (3)$$

$$\frac{\partial g^{mod}(At^2)}{\partial t} = \frac{-4At}{2(1+8At^2)^{5/4}} + \frac{-40A^2t^3}{2(1+80A^2t^4)^{9/8}} \quad (4)$$

$$\frac{\partial g_\infty^{mod}(\zeta=0,s)}{\partial s} = \frac{-4\chi_\infty s}{2(1+8\chi_\infty s^2)^{5/4}} + \frac{-40\chi_\infty^2 s^3}{2(1+80\chi_\infty^2 s^4)^{9/8}} \quad (5)$$

Although the SCAN functional reproduces the exact exchange-correlation energy of the helium atom [E_{XC}(SCAN) = -1.068 a.u. and E_{XC}(exact) = -1.068 a.u.] on the exact electron density, it does not reproduce the exchange and correlation parts separately [E_X(SCAN) = -1.02953 a.u. and E_C(SCAN) = -0.03847 a.u., while E_X(exact) = -1.026 a.u. and E_C(exact) = -0.042 a.u.]. In this paper, we also discuss the possibility of reproducing both the exchange and correlation energies of the helium atom separately. Since the single-orbital exchange part contains only two variables, and one of them is needed to normalize the single-orbital exchange for the exchange energy of the hydrogen atom, we could gain some flexibility in the exchange releasing the suggested local tighter upper bound for the single-orbital exchange enhancement factor ($F_X \leq 1.174$). Note that releasing this bound locally does not lead to the violation of this bound globally for any of the two-electron systems examined here (*vide infra*).

For all the calculations, we used the MRCC quantum chemistry software[40] with a modified development version of the *Libxc 3.0.1* density functional library.[41] We computed the electron densities of atomic (He, Li^+, Be^{2+}, B^{3+}, C^{4+}, N^{5+}, O^{6+}, F^{7+}, Ne^{8+})[42] and molecular [H_2,[43] HeH^+,[44] He_2^{2+},[45] H_3^+(linear),[46] H_3^+(triangle),[47] H_4^{2+}(square),[46] and H_4^{2+}(tetrahedral)[46] with experimental or calculated geometries presented in Table S1 of the supporting information] two-electron spin-singlet systems and tested the modifications in the prototype functionals considering the size-intensive normed integral absolute deviation (NIAD)[48] of the computed electron densities, gradients, and Laplacians from the reference composite coupled-cluster singles, doubles, triples, and quadruples (CCSDTQ)/aug-cc-pwCV5Z densities, gradients, and Laplacians.[48]

For testing purposes, we also used the electron densities of several spin-singlet many-electron atoms (Be, B^+, C^{2+}, N^{3+}, O^{4+}, F^{5+}, Ne^{6+}, Ne) and molecules (LiH, Li_2, LiF, BH_3, H_2O, HF, CO, N_2, F_2) with composite CCSDTQ/aug-cc-pwCV5Z reference densities again.[48] For the electron density calculations and the AE6 atomization energy test set,[49,50] we applied the aug-cc-pV5Z basis set[51] for the hydrogen and helium atoms and the very large aug-cc-pwCV5Z basis set[52] for the heavy atoms. For the potential energy of the compressed argon dimer at 1.6, 1.8, and 2.0 Å distances, we used the aug-cc-pwCV5Z basis set and accurate *ab initio* reference values.[53] For the calculation of the single-point energies of the noble gas atoms, we applied the UGBS basis set.[54] For the W4 atomization energy test set,[55] we used the def2-QZVPP basis set and the def2-QZVPP-RI-JK density fitting basis set.[56,57] For the G2RC reaction energy test set,[58] we applied the aug-cc-pVQZ basis set[51] with the aug-cc-pVQZ-RI-JK auxiliary basis set.[59] For the DBH24 reaction barrier test set,[55,60,61] the aug-cc-pVTZ basis set[51] was used with the aug-cc-pVTZ-RI-JK auxiliary basis set.[59] For the S22x5 test set,[62] we applied the aug-cc-pVTZ basis set,[51] the aug-cc-pVTZ-RI-JK auxiliary basis set,[59] as well as the counterpoise (CP) correction.[63]

Parameter determination

In the single-orbital exchange part, we examined the possibility of reproducing the exact exchange energies of the hydrogen (E_X = -0.3125 a.u.) and helium (E_X = -1.026 a.u.) atoms at the same time locally releasing the tighter lower bound and resetting the parameters to h_X^0 = 1.2755 and a_1 = 2.26161 (for the functional form and the parameter definitions, please see ref 31). We will call this the reparametrized SCAN exchange. In the single-orbital correlation part (with either the original or the revised SCAN correlation functional form), we have determined the value of the b_{1C} parameter to set the high-density limit of the correlation energy of the two-electron ions to its exact value (E_C = -0.046663 a.u.). We have chosen the value of the b_{3C} parameter to ensure that the single-orbital $F_{XC} \leq 1.67082$ even

for the low-density limit of the homogeneous electron gas. We have selected the value of the b_{2C} parameter to set the correlation energy of the helium atom to its exact value (E_C = -0.042 a.u.).

The first prototype, p1-revSCAN, is constructed from the original SCAN exchange + revised SCAN correlation with b_{1C} = 0.030197, b_{2C} = 0.06623, b_{3C} = 0.16672. The second prototype, p2-revSCAN, is assembled from the reparametrized SCAN exchange + reparametrized SCAN correlation with b_{1C} = 0.0285515, b_{2C} = -0.07248, b_{3C} = 0.15764. The third prototype, p3-revSCAN, includes the reparametrized SCAN exchange + revised SCAN correlation (with PBE-like fourth-order behavior) with b_{1C} = 0.030197, b_{2C} = -0.07955, b_{3C} = 0.16672. These prototypes are not ready for general use, but serve as starting point for further optimizations.

For a general purpose functional, the parameters k_1, c_{1x}, c_{2x}, d_x, c_{1c}, c_{2c}, and d_c should be refitted. In the fitting procedure applied in the original SCAN paper, these seven parameters were chosen to satisfy the large-Z limit of the exchange and correlation of noble gas atoms as well as considering jellium surface exchange-correlation energies, the potential energy of the compressed argon dimer, and the krypton atom as a unified atom limit. We use here a somewhat simpler procedure fitting the parameters for the six atomization energies of the AE6 test set preserving the correct large-Z limit of the exchange and correlation of noble gas atoms as well as extrapolating the exchange and correlation energies together to the $\alpha \to \infty$ limit with $d_x = d_c$. Our goal in this paper is to test the above mentioned ideas on simple single-orbital systems and discuss their applicability in a general purpose functional.

Results and discussion

The computed average NIADs for the electron density, gradient, and Laplacian are presented in Table 1 (the individual NIADs are in Tables S2 and S3). For the atomic densities, the largest improvement with the p1-revSCAN functional (with SCAN exchange and revised SCAN correlation) compared to the original SCAN functional is 5.5% appearing at the He atom, while the improvement is only 0.8% for the Ne^{8+} ion tending to be smaller towards the high-density limit. Similarly, the p1-revSCAN atomic density gradients are 0.6-4.0% more accurate, and the Laplacians are 0.4-2.9% better than the corresponding quantities obtained with SCAN. There is a large improvement in the computed atomic densities with the p2-revSCAN functional (with reparametrized SCAN exchange and SCAN correlation), which varies between 69-72%. Interestingly, the smallest improvement occurs at the He atom, and the largest improvement takes place for the Li^+ ion among the examined systems, otherwise at the high density limit, it seems to converge to 71%. The accuracy gain is between 68-73% in the gradients, and between 62-67% in the Laplacians with the p2-revSCAN atomic density gradients. The p3-revSCAN functional (with reparametrized SCAN exchange and revised SCAN correlation) shows an even larger improvement between 72-74% for computed atomic densities. Again, the improvements in the gradients and Laplacians are somewhat larger with the p3-revSCAN functional, they are between 70-75% as well as between 64-68%, respectively.

For the two-electron spin-singlet molecular systems, the electron density, gradient, and Laplacian are 1.4%, 1.6%, and 1.8% more accurate on average for the entire molecular test set with the p1-revSCAN functional. The largest improvement is 9.8% in the density, 7.6% in the gradient, and 5.7% in the Laplacian, and all of them occur for the neutral H_2 molecule. For the two-electron molecular cations, the errors are generally smaller with only one exception. The density of the linear H_3^+ molecule is slightly worse than the corresponding SCAN density, although the gradient and the Laplacian are slightly better. The p2-revSCAN electron densities are 1.4% worse, while the gradients and Laplacians are, in order, 8.5% and 6.6% better than the corresponding SCAN density derivatives on average. The electron densities of the H_2, HeH^+, H_3^+(triangle), and H_4^{2+}(tetrahedral) molecules are somewhat better, while those of the He_2^{2+}, H_3^+(linear), and H_4^{2+}(square) molecules are somewhat worse than the corresponding SCAN

densities. Note that among the H_3^+ and H_4^{2+} isomers, H_3^+(triangle) and H_4^{2+}(tetrahedral) are the most stable ones. There is again an improvement in the gradients of the H_2, HeH^+, H_3^+(triangle), and H_4^{2+}(tetrahedral) molecules and a deterioration in the gradients of the He_2^{2+}, H_3^+(linear), and H_4^{2+}(square) molecules. In the Laplacian, improvements can be observed at the HeH^+, H_3^+(triangle), and H_4^{2+}(tetrahedral) molecules, while the Laplacian errors are larger for the He_2^{2+}, H_3^+(linear), and H_4^{2+}(square) molecules and slightly larger for the H_2 molecule than the corresponding SCAN errors. The error pattern is quite similar with the p3-revSCAN functional. The density, gradient, and Laplacian errors are slightly larger than the corresponding p2-revSCAN errors for the two-electron spin-singlet molecular test set on average.

Next, we discuss the applicability of these modifications in a general purpose functional. Fitting the parameters k_1, c_{1x}, c_{2x}, d_x, c_{1c}, c_{2c}, and d_c for the AE6 test set, we managed to obtain accurate atomization energies with the p1-revSCAN functional form with the $k_1 = 0.065$, $c_{1x} = 0.607$, $c_{2x} = 0.7$, $d_x = d_c$, $c_{1c} = 1.131$, $c_{2c} = 1.7$, and $d_c = 1.37$ parameters (Table S4). We will call this general purpose functional revSCAN. For the AE6 test set, the root mean square deviation (RMSD) achieved by revSCAN is on par with that by the SCAN functional [RMSD(revSCAN) = 3.21 kcal mol^{-1}; RMSD(SCAN)=3.14 kcal mol^{-1}]. Note that the SCAN predictions are quite good, even though the SCAN functional was not fitted for any chemically bonded systems. In contrast, the revSCAN functional was fitted for the AE6 test set but preserving the same exact constraints that were used in the construction of the SCAN functional. For this reason, it gives similar results to the SCAN functional for the exchange and correlation energies of the noble gas atoms (Table S5). Although the revSCAN functional was not fitted for the potential energy of the compressed argon dimer, it shows somewhat more accurate results than the SCAN functional at smaller distances (Table S6). The revSCAN exchange results in 4-5 kcal mol^{-1} more repulsive interaction than the SCAN exchange, while the revSCAN correlation leads to 0.7-0.8 kcal mol^{-1} more attraction than the SCAN correlation. We assume that the observed more repulsive behavior of the revSCAN functional may be originated in the increased nonlocality of the revSCAN exchange in the noncovalent regions compared to the SCAN exchange [d_X(revSCAN) = 1.37 > d_X(SCAN) = 1.24].

In contrast to the p1-revSCAN functional form, we did not manage to obtain atomization energies comparable to the original SCAN functional in the functional forms based on our reparametrized exchange (*i.e.*, the p2- or p3-revSCAN), in spite of that the exchange enhancement factor of this reparametrized SCAN exchange energy globally satisfies the tighter lower bound for all the examined two-electron systems [$F_X = 1.162$ for the He atom, 1.166 for the large-Z limit of two-electron ions, and 1.168 for the H_2, 1.163 for the HeH^+, 1.161 for the He_2^{2+}, 1.166 for the H_3^+(linear), 1.173 for the H_3^+(triangle), 1.170 for the H_4^{2+}(square), and 1.174 for the H_4^{2+}(tetrahedral) molecules]. We conclude that locally releasing the tighter lower bound on the exchange in single-orbital regions leads to a large improvement in the single-orbital atomic regions which is, however, not accompanied by a similar improvement in the single-orbital molecular regions preventing these modified functional forms to be successful in the description of atomization energies. Furthermore, increasing the non-locality of the exchange (and removing the error cancellation between the exchange and correlation parts) in single-orbital regions may also cause a compatibility problem between the single-orbital and slowly-varying functional forms. The original SCAN exchange seems to be robust either paired with the original or modified SCAN correlation. Based on the above analysis, in our proposed revSCAN, we decided to keep the $F_X \leq 1.174$ exact condition for any single-orbital density. In the following, we will focus on the performance of the general purpose revSCAN functional based on the p1-revSCAN prototype.

Following the conclusion of Medvedev et al.[42] that density functional approximations should provide good electron densities and energetics at the same time, we have computed first the electron densities of several closed shell many-electron atoms with the SCAN and revSCAN functionals. The computed average NIADs for the electron density, gradient, and Laplacian are shown in Table 2 (the

individual NIADs are presented in Tables S7 and S8). The errors in the many-electron atomic electron densities and gradients are slightly smaller on average with the revSCAN functional than those with the SCAN functional, while the errors in the atomic density Laplacians are slightly larger on average. The largest differences between the two functionals occur for the neutral Be and Ne atoms, and this difference seems to decrease with increasing positive charge. The average errors in the many-electron molecular electron densities, gradients, and Laplacians are slightly larger with the revSCAN functional than those with the SCAN functional (please see Table 2). The largest differences between the two functionals occur for the BH_3 and N_2 molecules, while a slight improvement can be observed at the LiH and LiF molecules. Considering both the many-electron atomic and molecular electron densities, the revSCAN functional shows similar performance to the SCAN functional on average.

Next, we also tested the revSCAN functional on the W4 atomization energy test set containing the atomization energies of 99 molecules. The error distribution for this test set is shown in Figure 2 (the individual atomization energies can be found in Table S9). For the entire test set, the revSCAN functional shows somewhat better accuracy and precision than the SCAN functional, which can be followed by the mean (MD), mean absolute (MAD), and standard deviations (SD) from the reference (MD = -1.48 kcal mol^{-1}, MAD = 4.37 kcal mol^{-1}, SD = 5.95 kcal mol^{-1} for SCAN, as well as MD = -1.06 kcal mol^{-1}, MAD = 4.22 kcal mol^{-1}, SD = 5.55 kcal mol^{-1} for revSCAN). For the 16 systems with multireference character, the revSCAN functional is by 1 kcal mol^{-1} more accurate and considerably more precise on average than the original SCAN functional (MD = 1.17 kcal mol^{-1}, MAD = 6.92 kcal mol^{-1}, SD = 10.04 kcal mol^{-1} for SCAN, as well as MD = 0.16 kcal mol^{-1}, MAD = 5.91 kcal mol^{-1}, SD = 8.37 kcal mol^{-1} for revSCAN), while for the other systems without multireference character, the two functionals provide similar errors on average. For these systems, the revSCAN functional is somewhat more accurate but less precise than the SCAN functional (MD = -1.99 kcal mol^{-1}, MAD = 3.88 kcal mol^{-1}, SD = 4.71 kcal mol^{-1} for SCAN, as well as MD = -1.29 kcal mol^{-1}, MAD = 3.89 kcal mol^{-1}, SD = 4.86 kcal mol^{-1} for revSCAN). We also assessed the performance of the SCAN and revSCAN functionals on the G2RC reaction energy test set constituted of small systems, where dispersion interactions expectedly play only a marginal role. The individual errors for the 25 reactions are shown in Figure 3 (the individual reaction energies are presented in Table S10). For these reactions, the revSCAN functional is somewhat less accurate but more precise than the SCAN functional (MD = -2.83 kcal mol^{-1}, MAD = 6.46 kcal mol^{-1}, SD = 7.63 kcal mol-1 for SCAN, as well as MD = 3.82 kcal mol^{-1}, MAD = 6.01 kcal mol^{-1}, SD = 6.43 kcal mol^{-1} for revSCAN). Notice that the performance of the methods on atomization energies is related to their performance on reaction energies according to Hess's law.

Semi-local functionals can work well for atomization energies if the exchange and correlation holes are both well-localized around the electron or the long-range part of the exchange and correlation holes cancel each other (so they can capture a part of the static correlation in systems with multi-reference character). However, as Sun et al. discussed in their paper,[31] semi-local functionals cannot and should not be accurate when the exchange-correlation hole is non-local. For instance, the description of non-covalent complexes requires a non-local correlation functional, as well as the description of reaction barrier heights needs a non-local exchange functional.

To take into account the dispersion interactions, we have fitted the non-local VV10 correction[64] to the revSCAN functional using the equilibrium complexes from the S22x5 test set. The optimal value of the *b* parameter is 9.8 for the revSCAN functional with RMSD = 0.50 kcal mol^{-1} for the equilibrium complexes. For comparison, the *b* parameter is 14.1[37] for the SCAN functional with RMSD = 0.67 kcal mol^{-1} for the equilibrium complexes. (The obtained smaller *b* parameter in revSCAN-VV10 agree well with our earlier observation on the compressed argon dimer that revSCAN leads to more repulsive interaction at short-range than SCAN.) In Figure 4, we present the mean absolute deviations from the reference S22x5 interaction energies for the SCAN, revSCAN, SCAN-VV10, and revSCAN-VV10

methods for each distance and grouped by the dominating interaction type (please see Table S11 for the individual interaction energies). Without any dispersion correction, the revSCAN functional leads to generally less attractive interactions than the SCAN functional. This difference is especially large at shorter distances; however, it looks like that, for the same reason, the revSCAN functional can be corrected better than the SCAN functional with an appropriate dispersion correction. The SCAN-VV10 method overestimates more the interaction energies at short distances on average than the revSCAN-VV10 method. Note that the largest difference between the SCAN and revSCAN interaction energies can be found for the dispersion dominated complexes, while the largest improvement with revSCAN-VV10 occurs for the hydrogen-bonded complexes, where the dispersion interaction is smaller in magnitude. We assume that partially recovering the missing dispersion interaction at medium range by the semi-local exchange-correlation might lead to a double counting of this interaction in the SCAN-VV10 method. The revSCAN-VV10 functional is slightly less accurate at large distances, but the improvement at short distances is more significant, hence the latter method is more accurate for all types of interactions in this test set on average. The MAD values for the revSCAN-VV10 method are 0.40 kcal mol^{-1} for the hydrogen-bonded complexes, 0.25 kcal mol^{-1} for the dispersion dominated complexes, 0.25 kcal mol^{-1} for the mixed interaction complexes, and 0.30 kcal mol^{-1} for the entire test set, while the MAD values for the SCAN-VV10 method are 0.54 kcal mol^{-1}, 0.28 kcal mol^{-1}, 0.27 kcal mol^{-1}, and 0.36 kcal mol^{-1}, respectively.

To take into account the non-locality of the exchange hole in the calculations of reaction barrier heights, we considered hybridizing the semi-local revSCAN exchange with exact exchange in a global hybrid form. Note that the optimal exact exchange mixing varies with the systems and properties under consideration. We examined various exact exchange ratios in our revSCAN-based global hybrid form from 0% to 40% increasingly by 5% (Figure 5). The lowest MAD occurs at 35% of exact exchange for the barrier heights of the DBH24 test set, while at 20% of exact exchange for the 12 reaction energies of the same test set. As a compromise, considering the average of the two MADs, the lowest average error occurs for the two properties at 25% of exact exchange. This ratio has also proved to be successful for various thermochemical problems in the PBE0 functional.[65] For these reasons, we apply 25% of exact exchange and use the PBE0-like notation for the resulting functional: revSCAN0. In the following, we assess the performances of the revSCAN0 and the similar SCAN0[66] global hybrid functionals.

The error distributions for the DBH24 reaction barrier height test set with the SCAN0 and revSCAN0 functionals (as well as with the SCAN and revSCAN functionals for comparison) are shown in Figure 6 grouped by the different reaction families (the individual barrier heights are presented in Table S12). The results show that the revSCAN0 functional is generally more accurate than the SCAN0 functional for each type of reaction barrier heights considered here. The mean absolute deviations for the revSCAN0 method are 3.57 kcal mol^{-1} for the hydrogen atom transfer reactions, 3.40 kcal mol^{-1} for the heavy-atom transfer reactions, 0.88 kcal mol^{-1} for the nucleophilic substitution reactions, 3.38 kcal mol^{-1} for the unimolecular and recombination reactions, and 2.81 kcal mol^{-1} for the entire test set, while the mean absolute deviations for the SCAN0 method are 4.11 kcal mol^{-1}, 5.02 kcal mol^{-1}, 1.77 kcal mol^{-1}, 3.47 kcal mol^{-1}, and 3.59 kcal mol^{-1}, respectively.

We also briefly discuss here the possibility of locally mixing the SCAN or revSCAN exchange with a non-conventional exact exchange energy density[67] in a local hybrid functional that may locally satisfy the strongly tightened lower bound derived for the exchange energy of single-orbital systems (for further details, please see the Appendix). Our previous results show that a single-orbital exchange functional has to locally satisfy this constraint to be locally compatible with the slowly-varying SCAN exchange functional. Computing the position dependent ratio of the non-conventional exact exchange energy density and the exchange energy density from the local density approximation for two one-electron systems (*i.e.*, for the hydrogen atom and for the hydrogen molecular cation at different bond

lengths), we show that no member from the examined non-conventional exact exchange energy density family satisfies this constraint locally; therefore, we assume that such non-conventional exact exchange energy densities could not be mixed with the SCAN or revSCAN exchange in a local hybrid functional without compatibility problems.

Conclusions

We examined various possibilities to improve upon the semi-local SCAN functional. First, we tested three prototype revised versions of the SCAN functional (*i.e.*, p1-, p2-, and p3-revSCAN) on two-electron spin-singlet atomic and molecular densities. In the p1-revSCAN functional, we used a modified SCAN correlation recovering the slowly-varying behavior of the PBE correlation in a wider range and preserving the rapidly-varying behavior of the SCAN correlation. In the p2-revSCAN functional, we used a reparametrized SCAN exchange locally releasing the strongly tightened lower bound on the exchange in single-orbital regions (but keeping that globally for all the examined two-electron systems) to reproduce the exact exchange energies of the hydrogen and helium atoms at the same time. In the p3-revSCAN functional, we used the modified SCAN correlation together with the reparametrized SCAN exchange. The p1-revSCAN functional results in slightly better densities for the two-electron atomic and molecular systems than the original SCAN functional, while the p2- and p3-revSCAN functionals with the reparametrized exchange provide much more accurate atomic densities, and somewhat more accurate molecular densities. Then, we considered the possibility of constructing general purpose functionals from these prototype functionals refitting the parameters of the exchange and correlation interpolation-extrapolation functions constrained by exact conditions, such as the correct large-Z behavior of the exchange and correlation energy for noble gas atoms. In the p1-revSCAN functional form, we obtained atomization energies on par with the SCAN atomization energies for the AE6 test set but we did not manage to reach the accuracy of the SCAN functional for atomization energies with the p2- and p3-revSCAN functionals. This may be because the modified SCAN correlation leads to a slight but general improvement in the electron densities of two-electron atoms and molecules; however, the reparametrized SCAN exchange leads to a large improvement only in the atomic densities, which is not accompanied by a similar improvement in the molecular densities. Finally, we decided to keep the $F_X \leq 1.174$ exact condition for any single-orbital density in our general purpose functional denoted by revSCAN based on the p1-revSCAN prototype.

The proposed revSCAN functional provides slightly better many-electron atomic densities and slightly worse many-electron molecular densities than the SCAN functional. The revSCAN functional yields more accurate atomization energies for the molecular systems with multi-reference character and somewhat better precision for the reaction energies of small systems than the SCAN functional. To take into account the non-locality of the correlation in non-covalent complexes, we also fitted a non-local VV10 dispersion correction to the revSCAN functional and obtained more accurate interaction energies for the S22x5 test set with the revSCAN-VV10 method than with SCAN-VV10, especially for the hydrogen-bonded complexes and at smaller distances. To take into account the non-locality of the exchange in activated complexes, we hybridized the semi-local revSCAN exchange with exact exchange using a global hybrid functional form with 25% of exact exchange and obtained more accurate reaction barrier heights with the resulting revSCAN0 method than with the similar SCAN0 approach. We also considered locally hybridizing the semi-local exchange with a non-conventional exact exchange energy density assumed to locally satisfy the strongly tightened lower bound on the exchange in single-orbital regions, but we have showed that this non-conventional exact exchange energy density does not locally satisfy this constraint, and thus expectedly it is not compatible with the SCAN or revSCAN exchange energy densities.

Acknowledgments

The authors are grateful for the financial support from the National Research, Development, and Innovation Office (NKFIH, Grant No. KKP126451). The computing time granted on the Hungarian HPC Infrastructure at NIIF Institute, Hungary, is gratefully acknowledged.

Supporting information

Geometries of the two-electron molecular systems as well as detailed results for the discussed methods. This information is available free of charge via the Internet at http://pubs.acs.org/.

Tables and Figures

Table 1 Average normed integral absolute deviations (NIAD) of the computed two-electron atomic and molecular densities, gradients, and Laplacians from the reference for the original SCAN and the modified prototype functionals

	Atomic systems				Molecular systems			
	SCAN	p1-revSCAN	p2-revSCAN	p3-revSCAN	SCAN	p1-revSCAN	p2-revSCAN	p3-revSCAN
Density	0.0038	0.0037	0.0011	0.0010	0.0123	0.0122	0.0125	0.0128
Gradient	0.0353	0.0348	0.0099	0.0094	0.0365	0.0360	0.0334	0.0339
Laplacian	0.4512	0.4481	0.1506	0.1465	0.1155	0.1135	0.1079	0.1083

Table 2 Average normed integral absolute deviations (NIAD) of the computed many-electron atomic and molecular densities, gradients, and Laplacians from the reference for the SCAN and revSCAN functionals

	Atomic systems		Molecular systems	
	SCAN	revSCAN	SCAN	revSCAN
Density	0.0118	0.0115	0.0046	0.0057
Gradient	0.0582	0.0570	0.0189	0.0210
Laplacian	0.4629	0.4787	0.1810	0.2015

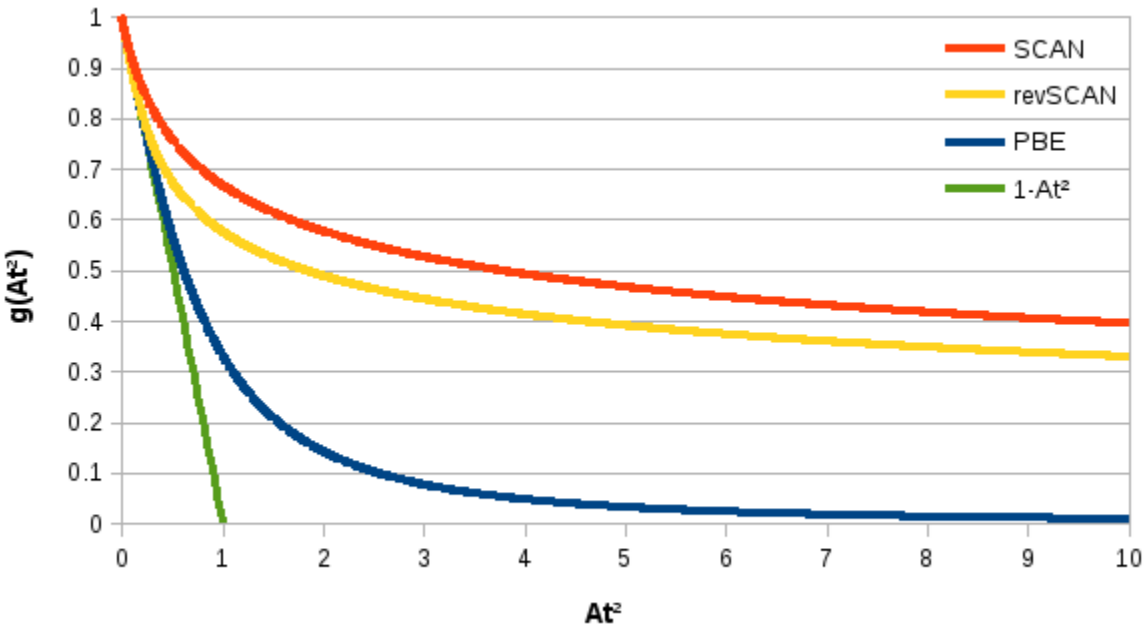

Figure 1 *The g function in the SCAN, revSCAN, and PBE correlation functionals*

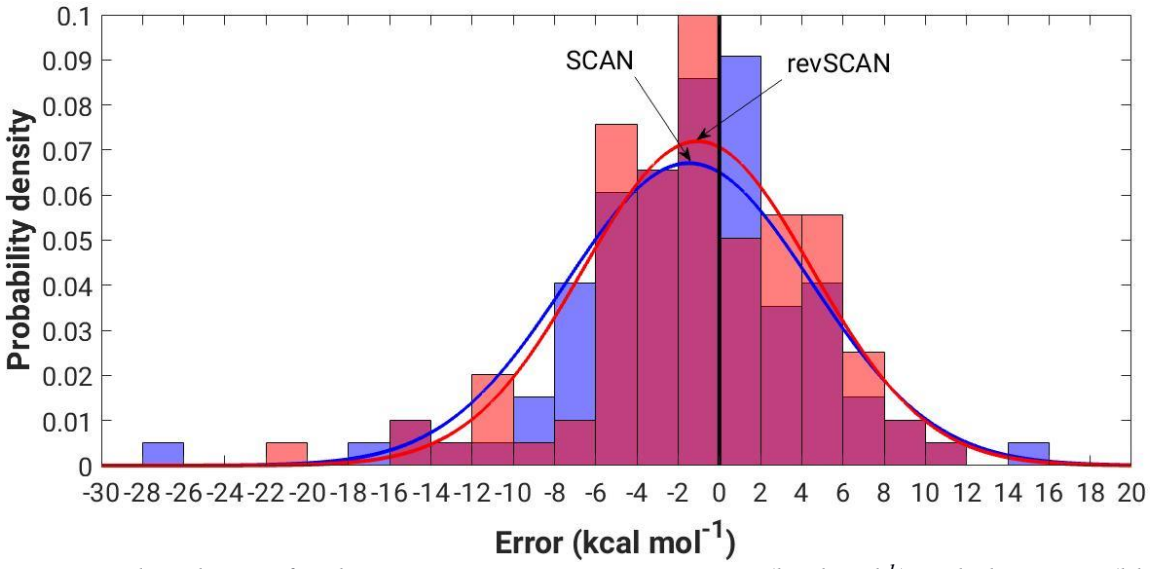

Figure 2 *Error distribution for the W4 atomization energy test set (kcal mol^{-1}) with the SCAN (blue curve) and revSCAN (red curve) functionals. (The light blue bars correspond to the histogram of SCAN, the pink bars correspond to the histogram of revSCAN, as well as the purple regions indicate the overlap between the light blue and pink bars.)*

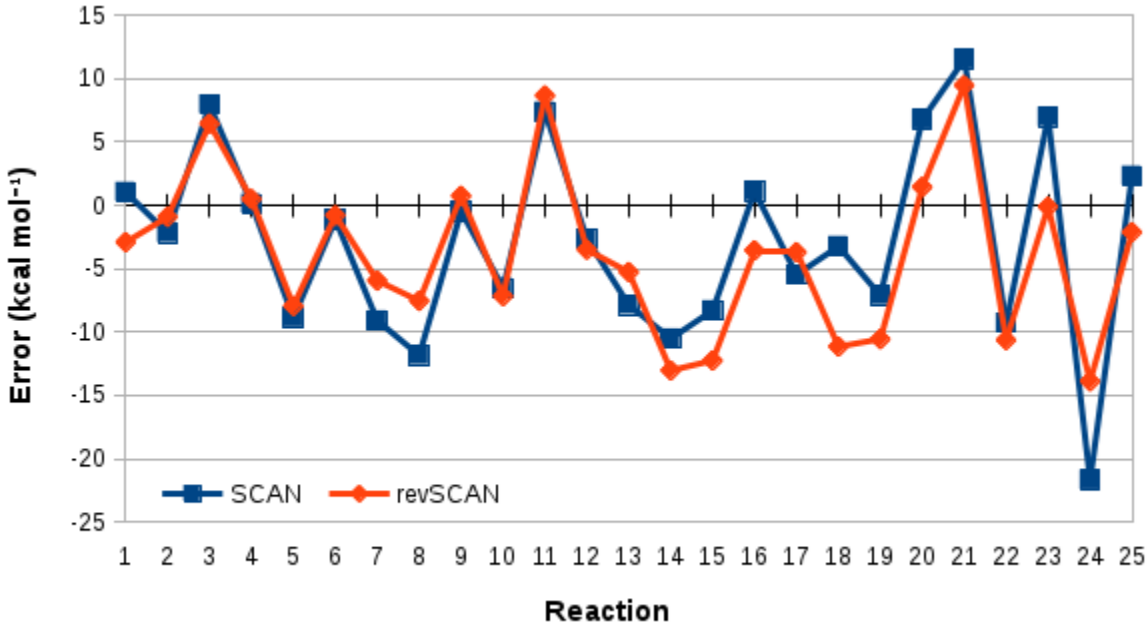

Figure 3 *Errors for the G2RC reaction energy test set (kcal mol^{-1}) with the SCAN and revSCAN functionals*

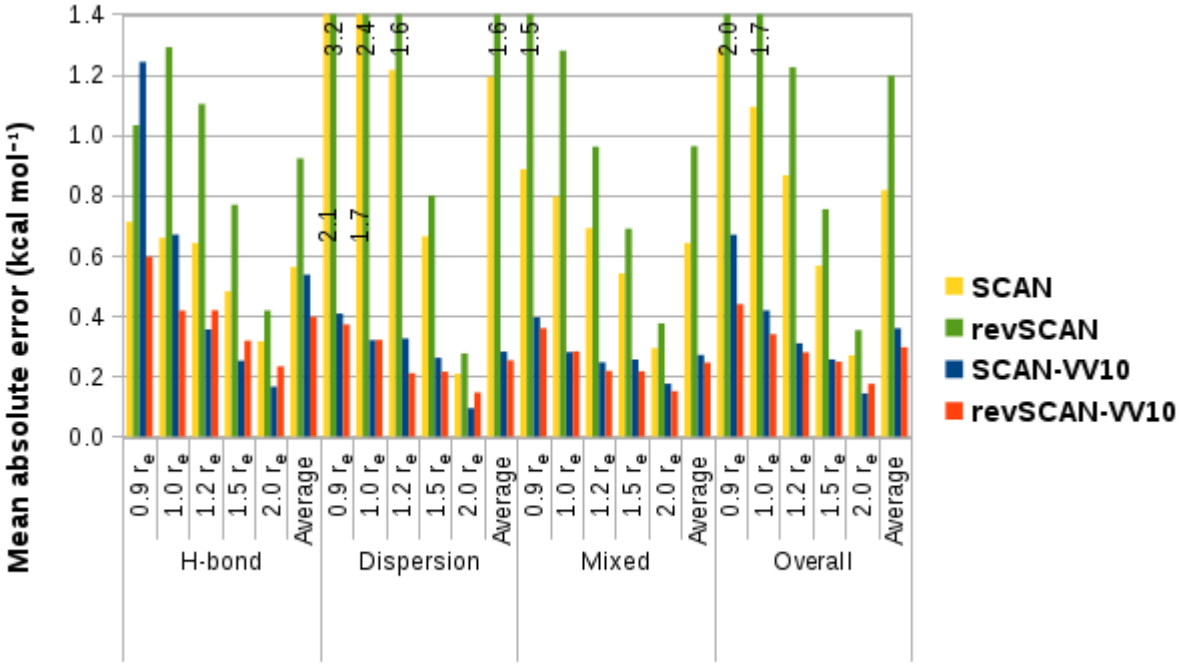

Figure 4 Mean absolute deviations from the reference S22x5 non-covalent interaction energies (kcal mol^{-1}) for the SCAN-VV10 and revSCAN-VV10 methods. (The outlying values are shown in the center of the diagram for SCAN-VV10, and on the top of the diagram for revSCAN-VV10. r_e stands for the unscaled equilibrium distance.)

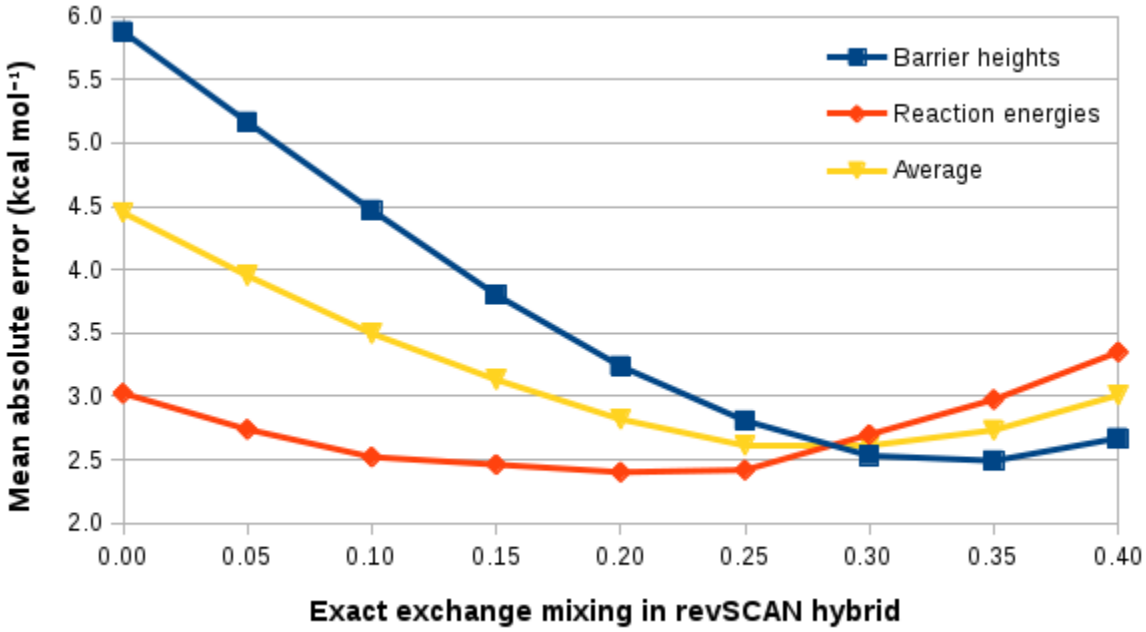

Figure 5 Mean absolute errors (kcal mol^{-1}) for the barrier heights and reaction energies of the DBH24 test set as well as the average of these two errors with respect to the exact exchange mixing ratio in the revSCAN global hybrid form

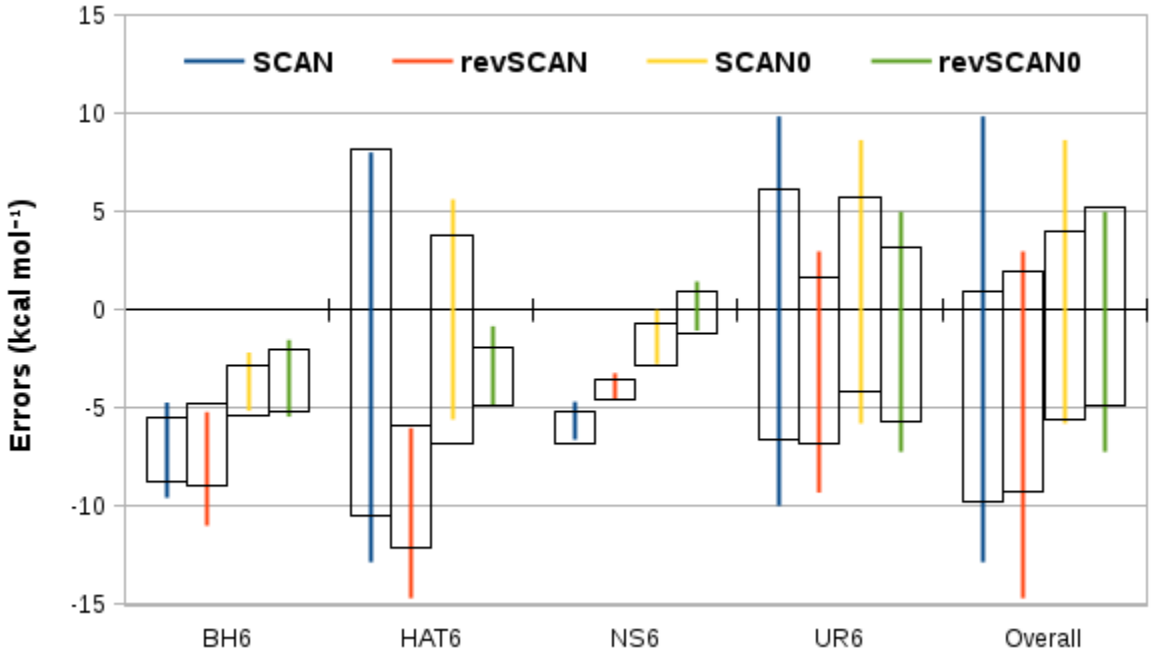

Figure 6 Errors in the DBH24 reaction barrier heights (kcal mol^{-1}) for the SCAN, revSCAN, SCAN0, and revSCAN0 functionals. (The vertical lines represent the error ranges, while the boxes represent the one standard deviation range around the mean errors. The subsets are: BH6 – hydrogen atom transfer reactions, HAT6 – heavy-atom transfer reactions, NS6 – nucleophilic substitution reactions, UR6 – unimolecular and recombination reactions.)

Appendix

The optimal bound for spin-polarized one-electron densities provided by Gadre et al.[30] is:

$$E_X[n_1] \geq -1.092 \int n_1^{4/3}(\boldsymbol{r}) d^3\boldsymbol{r} \quad , \tag{A-1}$$

where the exact exchange energy is a pure self-interaction correction, and n_1 is any one-electron density. This implies that a semi-local spin-unpolarized exchange enhancement factor should be globally lower than or equal to 1.174 for any single-orbital system. Perdew et al.[67] also suggested the existence of an exact exchange energy density generated by a simple coordinate transformation that locally satisfies this bound for a cuspless two-electron density. Even though the exchange energy density is non-unique and nonphysical, and it is the integrated exchange and correlation energies that should satisfy exact constraints, such exact exchange energy density may be relevant in the construction of a local hybrid functional based on the SCAN or revSCAN semi-local functionals.

In this appendix, we examine the suggested family of exact exchange densities (e_X^λ) that was used by Perdew et al.[67] to present a suggestive but inconclusive evidence for the existence of such exact exchange energy density. This family of exact exchange densities can be obtained by the following coordinate transformation:

$$e_X^\lambda(\boldsymbol{r}) = -\frac{1}{4}\int d^3\boldsymbol{u} \frac{|\rho(\boldsymbol{r}+\lambda\boldsymbol{u}, \boldsymbol{r}-[1-\lambda]\boldsymbol{u})|^2}{u} \quad , \tag{A-2}$$

where the density matrix can be calculated as $\rho(\boldsymbol{r},\boldsymbol{r}') = \sum_\sigma \sum_i^{occ} \psi_{i\sigma}^*(\boldsymbol{r})\psi_{i\sigma}(\boldsymbol{r}')$ with the $\psi_{i\sigma}$ spin-orbitals. The fully spin-polarized exact exchange energy densities ($e_{X,pol}^\lambda$) can be obtained applying the exact spin-scaling formula, $e_X[n_\alpha, n_\beta] = \left(e_X[2n_\alpha] + e_X[2n_\beta]\right)/2$, on the spin-unpolarized exact

exchange energy densities. For one-electron systems, this formula can be rewritten with the one-electron densities, $n_1(\boldsymbol{r}) = \psi_1^2(\boldsymbol{r})$, where ψ_1 is the only occupied one-electron orbital.

$$e_{X,pol}^{\lambda}(\boldsymbol{r}) = -\frac{1}{2}\int d^3\boldsymbol{u}\,\frac{|\rho(\boldsymbol{r}+\lambda\boldsymbol{u},\boldsymbol{r}-[1-\lambda]\boldsymbol{u})|^2}{u} \xrightarrow{1e^-} -\frac{1}{2}\int d^3\boldsymbol{u}\,\frac{n_1(\boldsymbol{r}+\lambda\boldsymbol{u})n_1(\boldsymbol{r}-(1-\lambda)\boldsymbol{u})}{u} \quad \text{(A-3)}$$

Albeit the concept of enhancement factors is introduced only for semi-local functionals, formally, effective position-dependent (fully spin-polarized) exact exchange enhancement factors ($F_{X,pol}^{\lambda}$) can be defined, as it was done by Perdew et al.,[67] for a given system dividing $e_{X,pol}^{\lambda}$ by the local density approximation (LDA) exchange energy density (e_X^{LDA}) to simply visualize if the exact exchange energy densities locally satisfy the suggested tighter lower bound:

$$F_{X,pol}^{\lambda}(\boldsymbol{r}) = \frac{e_{X,pol}^{\lambda}(\boldsymbol{r})}{e_X^{LDA}(\boldsymbol{r})} \quad . \quad \text{(A-4)}$$

Generally, the spin-unpolarized exact exchange enhancement factor can be obtained from the fully spin-polarized one by the following transformation:

$$F_{X,pol}(s) = 2^{1/3}F_X\left(s/2^{1/3}\right) \quad , \quad \text{(A-5)}$$

where s is the reduced gradient.

Since our question here is whether the suggested non-conventional exact exchange energy density is locally compatible with the semi-local SCAN or revSCAN exchange, we plot the position-dependent effective exact exchange enhancement factors with respect to the reduced gradient and apply a formally analog expression to transform the effective spin-polarized exact exchange enhancement factors into spin-unpolarized ones to facilitate the comparison with the SCAN or revSCAN semi-local (spin-unpolarized) exchange enhancement factors.

We consider simple prototypical one-electron systems to map how the suggested exact exchange energy densities behave in one-electron atomic regions, bonding regions, and for delocalized densities. Our first model is the hydrogen atom with the 1s orbital:

$$\psi_1(\boldsymbol{r}) = \frac{1}{\sqrt{\pi}}e^{-|\boldsymbol{r}|} \quad . \quad \text{(A-6)}$$

Then we model the hydrogen molecular ion (H_2^+) at various bond lengths using a simple approximate wave function form in prolate spheroidal coordinates to facilitate the calculations:[68]

$$\psi_1(\sigma,\tau) \approx c(1+\sigma)^{\frac{R}{a}-1}e^{-a\sigma}\cosh(b\tau) \quad , \quad \text{(A-7)}$$

where the coordinates $\sigma = (d_1 + d_2)/R$ and $\tau = (d_1 - d_2)/R$ can be obtained from the distances to the nuclei (d_1, d_2) and from the bond length (R). The corresponding parameter values can be found in ***Table A-1***.

Table A-1 Parameters for the approximate solution of the stretched hydrogen molecular ion (H_2^+)

R **(a.u.)**	***a***	***b***	***c***
0.2	0.1964	0.1135	1.5112
0.6	0.5483	0.3197	1.3230
1.0	0.8511	0.5034	1.2096
1.4	1.1200	0.6741	1.1418
2.0	1.4815	0.9192	1.0850
2.4	1.7035	1.0808	1.0636

For the hydrogen atom (***Figure A-1***), the effective exact exchange enhancement factors generated by coordinate transformation with $0.85 < \lambda < 1.00$ seem to diverge in the tail. However, others obtained by coordinate transformation with $0.50 \leq \lambda < 0.85$ are bounded from above. While the effective

conventional exact exchange enhancement factor monotonically grows with the reduced gradient, a maximum appears on the function in the range of $0.50 \leq \lambda < 0.85$. The maximum value on the $\lambda = 0.85$ curve is 1.204, which slightly violates the tighter upper bound ($F_X \leq 1.174$) suggested for one- and two-electron systems. This value further increases as λ approaches 0.50.

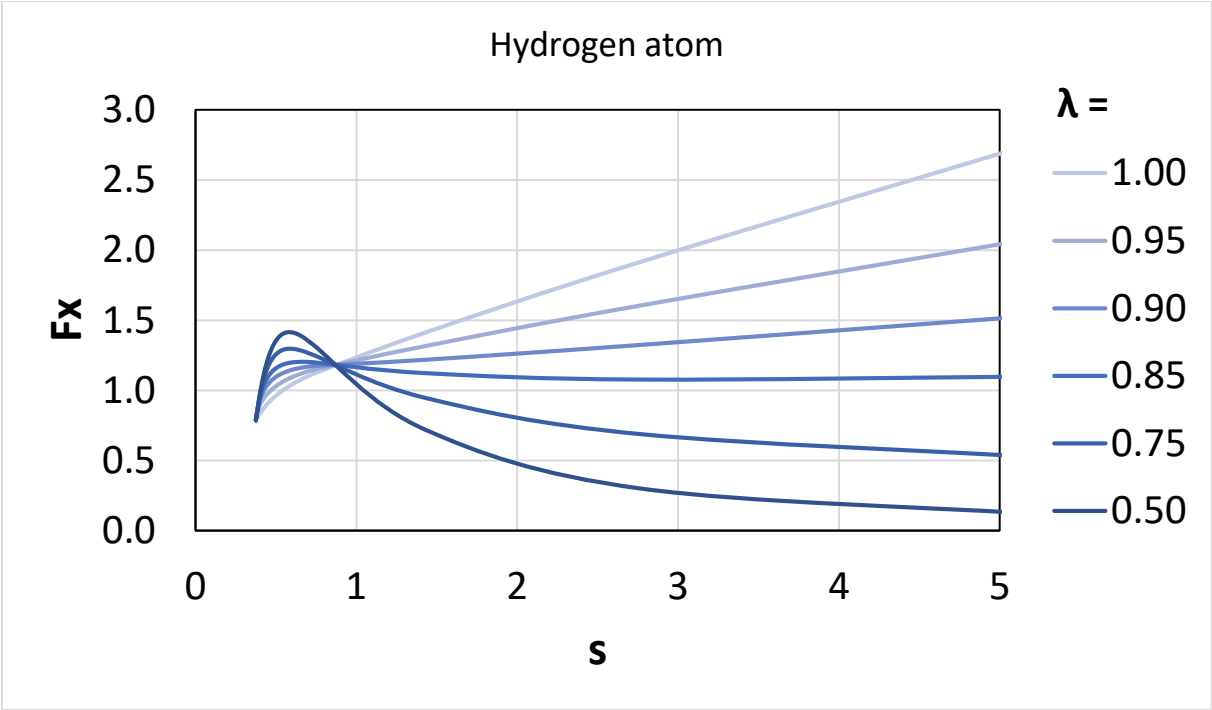

Figure A-1 Effective λ-dependent spin-unpolarized exact exchange enhancement factor for the hydrogen atom

For the equilibrium hydrogen molecular ion (***Figure A-2***), we represent the non-system-averaged effective exact exchange enhancement factors by two limiting cases: the points in the symmetry plane perpendicular to the bond axis and the points along the bond axis. The upper limiting curves correspond to the former, the lower limiting curves correspond to the latter cases. These two curves meet only at the bond critical point, where the reduced gradient is zero. The area between the upper and lower limiting curves belong to all the other spatial points. The horizontal part of the lower limiting curves corresponds to the nuclei, where the reduced gradient shows a discontinuity. The effective exact exchange enhancement factor of the equilibrium hydrogen molecular ion is upper bounded again in the range of $0.50 \leq \lambda < 0.85$. In the $\lambda = 0.85$ coordinate transformation, it violates the suggested tighter upper bound ($F_X \leq 1.174$) the most significantly at the bond critical point ($F_X = 1.473$). As λ approaches 0.50, the effective exact exchange enhancement factor increases in the bonding region and decreases in the asymptotic region.

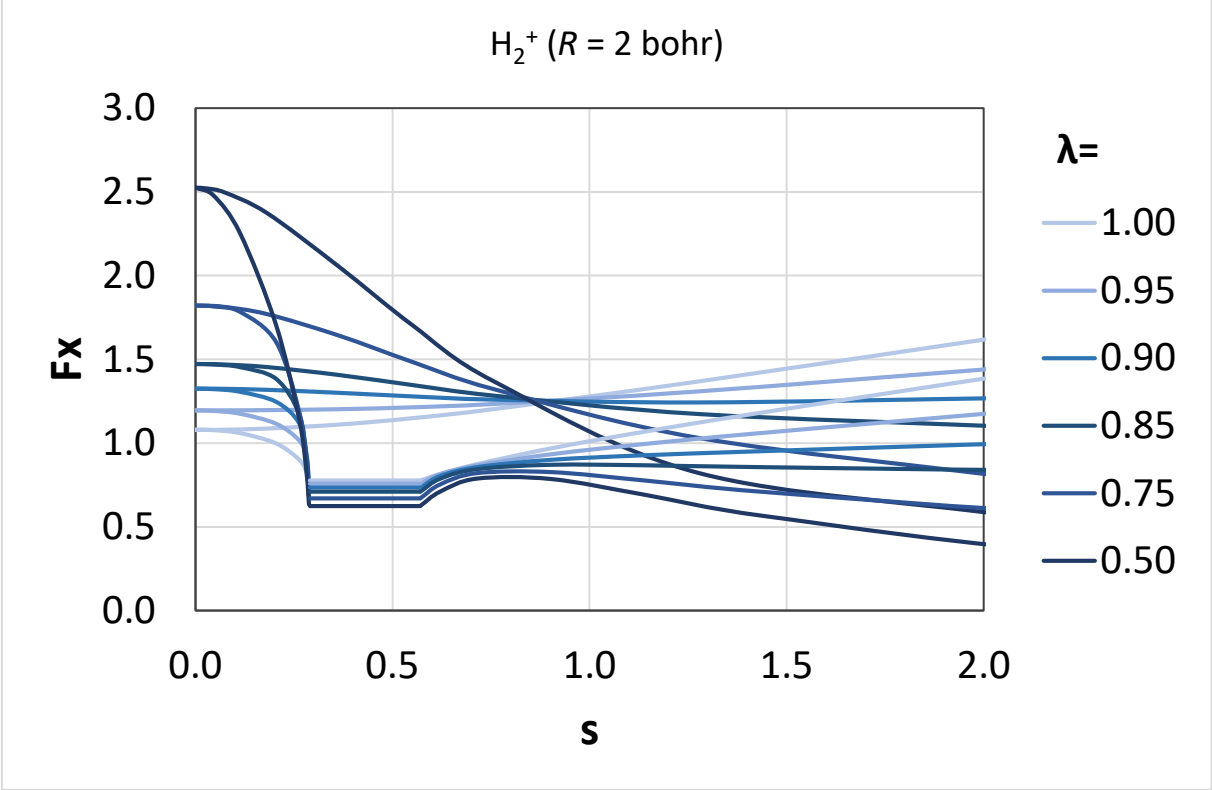

Figure A-2 Effective λ-dependent spin-unpolarized exact exchange enhancement factor for the approximate solution of the hydrogen molecular ion (H_2^+)

Increasing the bond length (***Figure A-3***) and thus the delocalization of the exact exchange hole, the bounded effective exact exchange enhancement factor in the λ = 0.85 coordinate transformation is increasing near the bond critical point and decreasing near the nuclei. (Note that the effective exact exchange enhancement factors in the unified atom limit of the hydrogen molecular ion are determined by the corresponding effective exact exchange enhancement factors of the hydrogen atom because of the uniform density scaling.) The larger the bond length, the more significantly this non-conventional effective exact exchange enhancement factor violates the suggested tighter upper bound ($F_X \leq 1.174$). For the bond lengths larger than 1 bohr, the maximum of the effective exact exchange enhancement factor appears at the bond critical point in this gauge.

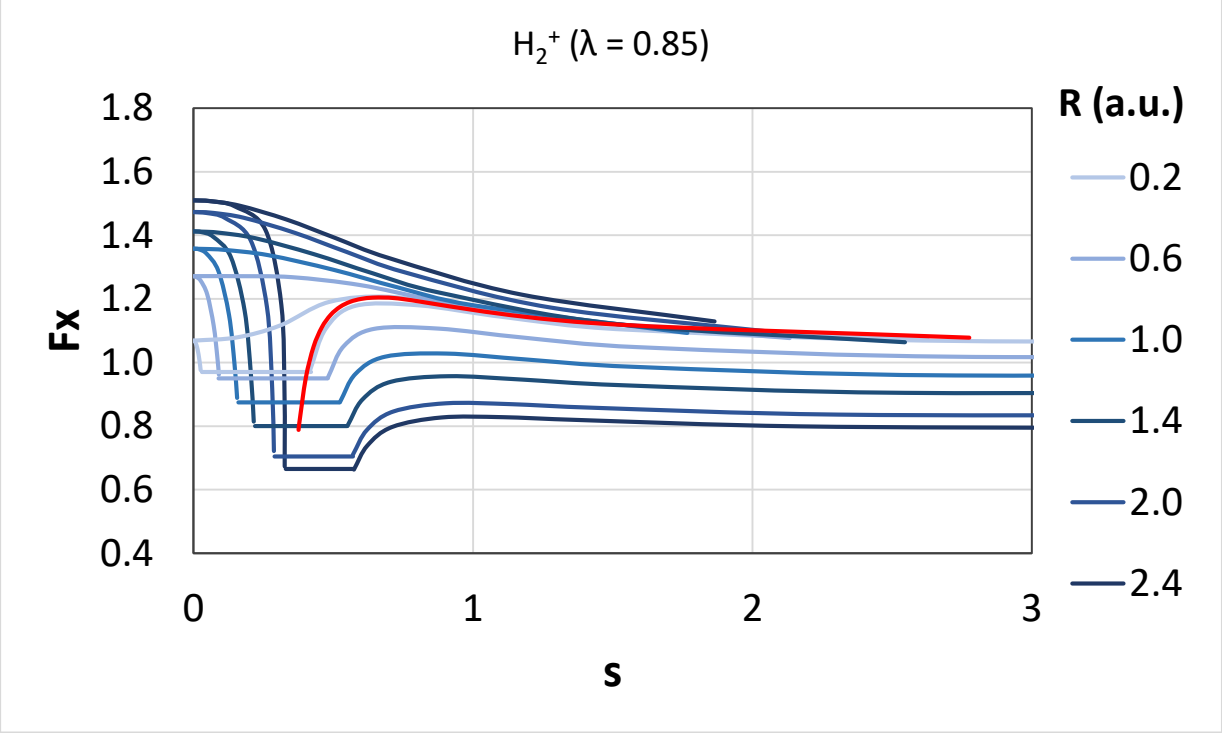

Figure A-3 Effective spin-unpolarized exact exchange enhancement factors generated by coordinate transformation with λ = 0.85 for the approximate solution of the stretched hydrogen molecular ion (H_2^+) at various bond lengths (red line: exact F_X for hydrogen atom).

References

[1] Becke, A. D. Fifty years of density-functional theory in chemical physics. *J. Chem. Phys.* **2014**, *140*, 18A301.
[2] Mardirossian, N.; Head-Gordon, M. Thirty years of density functional theory in computational chemistry: an overview and extensive assessment of 200 density functionals. *Mol. Phys.* **2017**, *115*, 2315-2372.
[3] Slater, J. C. A simplification of the Hartree-Fock method. *Phys. Rev.* **1951**, *81*, 385-390.
[4] Vosko, S. H.; Wilk, L.; Nusair, M. Accurate spin-dependent electron liquid correlation energies for local spin density calculations: a critical analysis. *Can J. Phys.* **1980**, *58*, 1200-1211.
[5] Perdew, J. P. Generalized gradient approximations for exchange and correlation: A look backward and forward. *Physica B* **1991**, *172*, 1-6.
[6] Burke, K.; Perdew, J. P.; Ernzerhof, M. Why the generalized gradient approximation works and how to go beyond it. *Int. J. Quantum Chem.* **1997**, *61*, 287-293.
[7] Mardirossian, N.; Head-Gordon, M. Mapping the genome of meta-generalized gradient approximation density functionals: The search for B97M-V. *J. Chem. Phys.* **2015**, *142*, 074111.
[8] Wang, Y.; Jin, X.; Yu, H. S.; Truhlar, D. G. Revised M06-L functional for improved accuracy on chemical reaction barrier heights, noncovalent interactions, and solid-state physics. *Proc. Natl. Acad. Sci.* **2017**, *114*, 8487-8492.
[9] Perdew, J. P.; Ruzsinszky, A.; Tao, J. Prescription for the design and selection of density functional approximations: More constraint satisfaction with fewer fits. *J. Chem. Phys.* **2005**, *123*, 062201.
[10] Zhao, Y.; Schultz, N. E.; Truhlar, D. G. Design of density functionals by combining the method of constraint satisfaction with parametrization for thermochemistry, thermochemical kinetics, and noncovalent interactions. *J. Chem. Theory Comput.* **2006**, *2*, 364-382.
[11] Perdew, J. P.; Burke, K.; Ernzerhof, M. Generalized gradient approximation made simple. *Phys. Rev. Lett.* **1996**, *77*, 3865-3868.
[12] Lieb, E. H.; Oxford, S. Improved lower bound on the indirect Coulomb energy. *Int. J. Quantum Chem.* **1981**, *19*, 427-439.
[13] Antoniewicz, P. R.; Kleinmann, L. Kohn-Sham exchange potential exact to first order in $\rho(K\rightarrow)/\rho_0$. *Phys. Rev. B* **1985**, *31*, 6779.
[14] Oliver, G. L.; Perdew, J. P. Spin-density gradient expansion for the kinetic energy. *Phys. Rev. A* **1979**, *20*, 397.
[15] Wang, Y.; Perdew, J. P. Spin scaling of the electron-gas correlation energy in the high-density limit. *Phys. Rev. B* **1991**, *43*, 8911.
[16] Levy, M. Asymptotic coordinate scaling bound for exchange-correlation energy in density-functional theory. *Int. J. Quantum Chem.* **1989**, *S23*, 617.
[17] Perdew, J. P.; Wang, Y. Accurate and simple analytic representation of the electron-gas correlation energy. *Phys. Rev. B* **1992**, *45*, 13244-13249.
[18] Perdew, J. P.; Ruzsinszky, A.; Csonka, G. I.; Vydrov, O. A.; Scuseria, G. E.; Constantin, L. A.; Zhou, X.; Burke, K. Restoring the density-gradient expansion for exchange in solids and surfaces. *Phys. Rev. Lett.* **2008**, *100*, 136406.
[19] Ruszinszky, A.; Csonka, G. I.; Scuseria, G. E. Regularized gradient expansion for atoms, molecules, and solids. *J. Chem. Theory Comput.* **2009**, *5*, 763-769.
[20] Zhang, Y.; Yang, W. Comment on "Generalized gradient approximation made simple". *Phys. Rev. Lett.* **1998**, *80*, 890.
[21] Hammer, B.; Hansen, L. B.; Nørskov, J. K. Improved adsorption energetics within density-functional theory using revised Perdew-Burke-Ernzerhof functionals. *Phys. Rev. B* **1999**, *59*, 7413-7421.
[22] Adamo, C.; Barone, V. Physically motivated density functionals with improved performances: The modified Perdew–Burke–Ernzerhof model. *J. Chem. Phys.* **2002**, *116*, 5933.
[23] Fabiano, E.; Constantin, L. A.; Della Sala, F. Generalized gradient approximation bridging the rapidly and slowly varying density regimes: A PBE-like functional for hybrid interfaces. *Phys. Rev. B* **2010**, *82*, 113104.
[24] Constantin, L. A.; Fabiano, E.; Laricchia, S.; Della Sala, F. Semiclassical neutral atom as a reference system in density functional theory. *Phys. Rev. Lett.* **2011**, *106*, 186406.
[25] del Campo, J. M.; Gázquez, J. L.; Trickey, S. B.; Vela, A. Non-empirical improvement of PBE and its hybrid PBE0 for general description of molecular properties. *J. Chem. Phys.* **2012**, *136*, 104108.
[26] Perdew, J. P.; Kurth, S.; Zupan, A.; Blaha, P. Accurate density functional with correct formal properties: A step beyond the generalized gradient approximation. *Phys. Rev. Lett.* **1999**, *82*, 2544-2547.
[27] Tao, J.; Perdew, J. P.; Staroverov, V. N.; Scuseria, G. E. Climbing the density functional ladder: Nonempirical meta–generalized gradient approximation designed for molecules and solids. *Phys. Rev. Lett.* **2003**, *91*, 146401.
[28] Svendsen, P. S.; von Barth, U. Gradient expansion of the exchange energy from second-order density response theory. *Phys. Rev. B* **1996**, *54*, 17402.
[29] Perdew, J. P.; Sun, J.; Ruzsinszky, A.; Mezei, P. D.; Csonka, G. I. Why Density Functionals Should Not Be Judged Primarily by Atomization Energies. *Period. Polytech. Chem. Eng.* **2016**, *60*, 2-7.

[30] Gadre, S. R.; Bartolotti, L. J.; Handy, N. C. Bounds for Coulomb energies. *J. Chem. Phys.* **1980**, *72*, 1034.
[31] Sun, J.; Ruzsinszky, A.; Perdew, J. P. Strongly constrained and appropriately normed semilocal density functional. *Phys. Rev. Lett.* **2015**, *115*, 036402.
[32] Sun, J.; Perdew, J. P.; Ruzsinszky, A. Semilocal density functional obeying a strongly tightened bound for exchange. *Proc. Natl. Acad. Sci.* **2015**, *112*, 685-689.
[33] Levy, M. Density-functional exchange correlation through coordinate scaling in adiabatic connection and correlation hole. *Phys. Rev. A* **1991**, *43*, 4637.
[34] Pollack, L.; Perdew, J. P. Evaluating density functional performance for the quasi-two-dimensional electron gas. *J. Phys. Condens. Matter* **2000**, *12*, 1239.
[35] Grimme, S.; Ehrlich, S.; Goerigk, L. Effect of the damping function in dispersion corrected density functional theory. *J. Comp. Chem.* **2011**, *32*, 1456-1465.
[36] Goerigk, L.; Hansen, A.; Bauer, C.; Ehrlich, S.; Najibi, A.; Grimme, S. A look at the density functional theory zoo with the advanced GMTKN55 database for general main group thermochemistry, kinetics and noncovalent interactions. *Phys. Chem. Chem. Phys.* **2017**, *19*, 32184-32215.
[37] Brandenburg, J. G.; Bates, J. E.; Sun, J.; Perdew, J. P. Benchmark tests of a strongly constrained semilocal functional with a long-range dispersion correction. *Phys. Rev. B* **2016**, *94*, 115144.
[38] Chen, M.; Ko, H-Y.; Remsing, R. C.; Andrade, M. F. C.; Santra, B.; Sun, Z.; Selloni A.; Car, R.; Klein, M. L.; Perdew, J. P.; Wu X. Ab initio theory and modeling of water. *Proc. Natl. Acad. Sci.* **2017**, *114*, 10846-10851.
[39] Sun, J.; Remsing, R. C.; Zhang, Y.; Sun, Z.; Ruzsinszky, A.; Peng, H.; Yang, Z.; Paul, A.; Waghmare, U.; Wu, X.; Klein, M. L.; Perdew, J. P. Accurate first-principles structures and energies of diversely bonded systems from an efficient density functional. *Nat. Chem.* **2016**, *8*, 831-836.
[40] MRCC, a quantum chemical program suite written by M. Kállay, Z. Rolik, J. Csontos, P. Nagy, G. Samu, D. Mester, J. Csóka, I. Ladjánszki, L. Szegedy, B. Ladóczki, K. Petrov, M. Farkas, and B. Hégely. See www.mrcc.hu.
[41] Marques, M. A. L.; Oliveira, M. J. T.; Burnus, T. Libxc: A library of exchange and correlation functionals for density functional theory. *Comput. Phys. Commun.* **2012**, *183*, 2272.
[42] Medvedev, M. G.; Bushimarinov, I. S.; Sun, J.; Perdew, J. P.; Lyssenko, K. A. Density functional theory is straying from the path toward the exact functional. *Science* **2017**, *355*, 49-52.
[43] NIST Computational Chemistry Comparison and Benchmark Database, NIST Standard Reference Database Number 101, Release 18, October 2016, Johnson, R. D., III, Ed. http://cccbdb.nist.gov/ (accessed March 30, 2017)
[44] Laaksonen, L.; Pyykkö, P.; Sundholm, D. Two-Dimensional fully numerical solutions of molecular Schrödinger equations. II. Solution of the Poisson equation and results for singlet states of H_2 and HeH^+. *Int. J. Quantum Chem.* **1983**, *XXIII*, 319-323.
[45] Ackermann, J.; Hogreve, H. On the metastability of the $^1\Sigma_g^+$ ground state of He_2^{2+} and Ne_2^{2+}: a case study of binding metamorphosis. *J. Phys. B* **1992**, *25*, 4069-4098.
[46] Frost, A. A. Floating spherical Gaussian orbital model of molecular structure. II. One- and two-electron-pair systems. *J. Chem. Phys.* **1967**, *47*, 3714.
[47] Porter, R. N. H_3 and H_3^+: Correlations of theory and experiment. *Ber. Bunsenges. Phys. Chem.* **1982**, *86*, 407-413.
[48] Mezei, P. D.; Csonka, G. I.; Kállay, M. Electron density errors and density-driven exchange-correlation energy errors in approximate density functional calculations. *J. Chem. Theory Comput.* **2017**, *13*, 4753-4764.
[49] Lynch, B. J.; Truhlar, D. G. Small representative benchmarks for thermochemical calculations. *J. Phys. Chem. A* **2003**, *107*, 8996.
[50] Haunschild, R.; Klopper, W. Theoretical reference values for the AE6 and BH6 test sets from explicitly correlated coupled-cluster theory. *Theor. Chem. Acc.* **2012**, *131*, 1112.
[51] Dunning, T. H. Gaussian basis sets for use in correlated molecular calculations. I. The atoms boron through neon and hydrogen. *J. Chem. Phys.* **1989**, *90*, 1007.
[52] Peterson, K. A.; Dunning Jr., T. H. Accurate correlation consistent basis sets for molecular core–valence correlation effects: The second row atoms Al-Ar, and the first row atoms B-Ne revisited. *J. Chem. Phys.* **2002**, *117*, 10548.
[53] Patkowski, K.; Murdachaew, G.; Fou, C-M.; Szalewicz, K. Accurate ab initio potential for argon dimer including highly repulsive region. *Mol. Phys.* **2005**, *103*, 2031-2045.
[54] de Castro, E. V. R.; Jorge, F. E. Accurate universal gaussian basis set for all atoms of the periodic table. *J. Chem. Phys.* **1998**, *108*, 5225.
[55] Karton, A.; Tarnopolsky, A.; Lamère, J.-F.; Schatz, G. C.; Martin, J. M. L. Highly accurate first-principles benchmark data sets for the parametrization and validation of density functional and other approximate methods. Derivation of a robust, generally applicable, double-hybrid functional for thermochemistry and thermochemical kinetics. *J. Phys. Chem. A* **2008**, *112*, 12868–12886.
[56] Weigend, F. Hartree-Fock exchange fitting basis sets for H to Rn. *J. Comput. Chem.* **2008**, *29*, 167-175.

[57] Weigend, F.; Ahlrichs, R. Balanced basis sets of split valence, triple zeta valence and quadruple zeta valence quality for H to Rn: Design and assessment of accuracy. *Phys. Chem. Chem. Phys.* **2005**, *7*, 3297-3305.
[58] Curtiss, L. A.; Raghavachari, K.; Redfern, P. C.; Pople, J. A. Assessment of Gaussian-2 and density functional theories for the computation of enthalpies of formation. *J. Chem. Phys.* **1997**, *106*, 1063-1079.
[59] Weigend, F. A fully direct RI-HF algorithm: Implementation, optimized auxiliary basis sets, demonstration of accuracy and efficiency. *Phys. Chem. Chem. Phys.* **2002**, *4*, 4285-4291.
[60] Zhao, Y.; Lynch, B. J.; Truhlar, D. G. Development and assessment of a new hybrid density functional model for thermochemical kinetics. *J. Phys. Chem. A* **2004**, *108*, 2715–2719.
[61] Zhao, Y.; González-García, N.; Truhlar, D. G. Benchmark database of barrier heights for heavy atom transfer, nucleophilic substitution, association, and unimolecular reactions and its use to test theoretical methods. *J. Phys. Chem. A* **2005**, *109*, 2012–2018.
[62] Gráfová, L.; Pitoňák, M.; Řezáč, J.; Hobza, P. Comparative study of selected wave function and density functional methods for noncovalent interaction energy calculations using the extended S22 data set. *J. Chem. Theory Comput.* **2010**, *6*, 2365–2376.
[63] Boys, S. F.; Bernardi, F. The calculation of small molecular interactions by the differences of separate total energies. Some procedures with reduced errors. *Mol. Phys.* **1970**, *19*, 553.
[64] Vydrov, O. A.; van Voorhis, T. Nonlocal van der Waals density functional: The simpler the better. *J. Chem. Phys.* **2010**, *133*, 244103.
[65] Adamo, C.; Barone, V. Toward reliable density functional methods without adjustable parameters: The PBE0 model. *J. Chem. Phys.* **1999**, *110*, 6158-6170.
[66] Hui, K.; Chai, J-D. SCAN-based hybrid and double-hybrid density functionals from models without fitted parameters. *J. Chem. Phys.* **2016**, *144*, 044114.
[67] Perdew, J. P.; Ruzsinszky, A.; Sun, J.; Burke, K. Gedanken densities and exact constraints in density functional theory. *J. Chem. Phys.* **2014**, *140*, 18A533.
[68] Weinhold, F. Variational Wavefunctions for H_2^+. *J. Chem. Phys*. **1972**, *56*, 3798-3801.

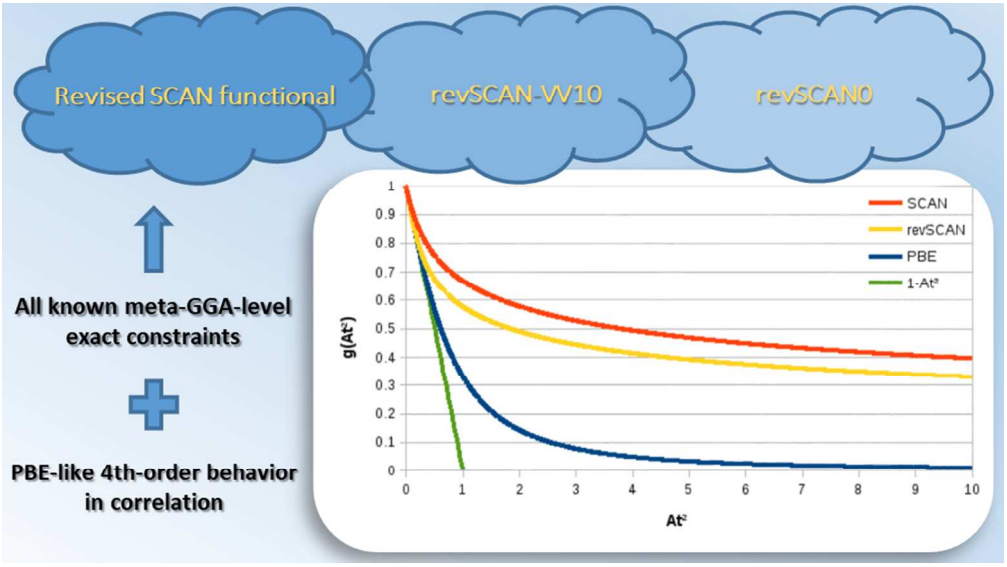

Revised SCAN functional

85x47mm (300 x 300 DPI)